Available online at www.sciencedirect.com
ScienceDirect
Mendeleev Commun., 2011, **21**, 125–128
Mendeleev Communications

Decoration of multiwall carbon nanotubes with nickel nanoparticles: effect of deposition strategy on metal dispersion and performance in the hydrogenation of *p*-chloroacetophenone

Miron V. Landau,*[a] Sergei V. Savilov,[b] Marina N. Kirikova,[b] Nikolai B. Cherkasov,[b] Anton S. Ivanov,[b] Valery V. Lunin,[b] Yuri Koltypin[c] and Aharon Gedanken[c]

[a] *Department of Chemical Engineering, Ben-Gurion University of the Negev, 84105 Beer-Sheva, Israel. Fax: +972 8 647 9427; e-mail: mlandau@bgu.ac.il*
[b] *Department of Chemistry, M. V. Lomonosov Moscow State University, 119991 Moscow, Russian Federation*
[c] *Department of Chemistry, Bar-Ilan University, 52900 Tel-Aviv, Israel*

DOI: 10.1016/j.mencom.2011.04.003

The sonochemical deposition of nickel nanoparticles onto the multiwall carbon nanotube aggregates leads to a uniformly distributed metal phase at high loadings and an average nickel crystal size of 4–8 nm at a 25–50 wt% nickel content. Its application enhances the catalytic activity of Ni/multiwall carbon nanotube material in the selective hydrogenation of chloroacetophenone by factors of 2–18, as compared with that prepared by traditional decoration methods.

Multiwall carbon nanotubes (MWCNTs) can be used as supports for nickel nanocrystals with controlled pore size distributions and surface areas and great thermal and chemical stability. They demonstrated wide opportunities in decoration of the outer surface of MWCNT[1–16] and/or filling their internal channels.[17,18] The synthesis of Ni/MWCNT composites by nickel-catalyzed decomposition of hydrocarbons gives a material with low metal loading where it is located mainly at the ends of nanotubes. In order to obtain appropriate catalysts, it is important to combine a small crystal size with a maximal metal loading.

In this study, different nickel deposition methods on MWCNT surfaces were compared. Sonochemical deposition from $Ni(CO)_4$ in decaline was used for the first time to prepare Ni/MWCNT composite with nickel size less than 10 nm under loadings of 25–50 wt%.†

Starting MWCNTs were obtained as bundles of nanotubes (external diameter, 30–80 nm) aggregates of ~2 μm size [Figure 1(*a*),(*b*)]. Nanotubes contained narrow empty channels with a diameter of 3–4 nm and formed voids as wider mesopores inside the aggregates. Nanotube walls consisted of parallel slightly disoriented graphene layers [Figure 1(*c*)], as confirmed by XRD after the removal of residual nickel, which occurred in the forms of metallic (Ni^0) and oxide (NiO) nanoparticles (Figure 2, curve *1*). It consumed hydrogen in the same temperature range as pure NiO (Figure 3, curves *2*, *3*). Nickel nanocrystals in sample S1 demonstrated size distribution of 20–100 nm and were located mainly at the ends of tubes [Figure 1(*b*)]. The average size was estimated at 30 nm from XRD data (Table 1).

The nickel content of sample S2, obtained by nickel deposition on purified carboxylated MWCNTs was 11 wt% according to chemical and XRD phase analysis with an average crystal size

† The MWCNTs with a diameter of 50–100 nm (sample S1) were synthesized by the pyrolysis of a benzene–ethanol solution of nickel acetylacetonate at 1000 °C.[12] After nickel extraction with 65% HNO_3, the surface of MWCNTs was carboxylated by treatment with H_2SO_4/HNO_3 (3:1, v/v) under sonication for 3 h at 40 °C followed by washing with water[19] and drying at 80 °C in air. MWCNT surface area was determined as 216±8 $m^2\ g^{-1}$. Carboxylated MWCNTs were decorated with metallic nickel by: (1) deposition of reducible Ni-containing precursors from aqueous solutions [1 M acetate (samples S2, S4) or formate (sample S3)] sonicated (20 kHz) at room temperature for 1 h followed by heating at 350 °C in nitrogen and reducing in an H_2 flow (100 $cm^3\ min^{-1}$) for 3 h at 550 °C (sample S2, S3). For sample S4 final reduction step after heating in nitrogen was conducted in 5% hydrazine hydrate in NaCl solution under sonication followed by treatment with an aqueous NaOH solution, washing with water and drying *in vacuo* at room temperature in a glove box.

Sonochemical deposition was done by sonication of carboxylated MWCNTs in $Ni(CO)_4$ solution in decalin with Ti-horn (20 kHz, 100 W cm^{-2}) sonicator (VCX 750, Sonics&Materials) under Ar at 5–10 °C for 3 h. The metal loading was controlled varying the concentration of metal precursor at the sonochemical deposition step in a range from 0.02 (sample S5) to 0.05 M (sample S6). For preparation of sample S7 the water–ethanol solution of nickel nitrate was added to MWCNTs at amount corresponding to their solution capacity. The material was heated at 350 °C in nitrogen and reduced in an H_2 flow (100 $cm^3\ min^{-1}$) for 3 h at 550 °C. H_2-TPR experiments were performed on AMI-100 (Zeton-Altamira Co.) equipped with a TCD detector at 10% H_2–Ar flow of 25 ml min^{-1} with gradual temperature increase of 5 K min^{-1}. Conventional wide-angle XRD patterns were obtained with a Philips 1050/70 powder diffractometer fitted with a graphite monochromator and Crystal Logic software. The nickel content of Ni/MWCNT-supported catalysts was calculated based on metal/carbon atomic ratios measured by energy-dispersive X-ray analysis spectroscopy (EDAX, Quanta-2000, SEM-EDAX, FEI Co) and by ICP method (Instrument Optima 3000, Perkin Elmer Co.) in the solution obtained after HNO_3 (70%) treatment. Adsorption-desorption isotherms were obtained with a NOVA-2000 (Quantachrome Inc., version 7.11) surface area analyzer. HRTEM analysis was conducted on a FasTEM JEOL 2010 microscope operating at 200 kV. Activity and selectivity of Ni/MWCNT catalysts was tested in hydrogenation of *p*-chloroacetophenone (PCAP), conducted in a 20 ml stainless steel batch reactor with internal Teflon coating equipped with a magnetic stirrer. The reduced or vacuum-dried (direct nickel deposition) catalysts were loaded in the glow box to the reactor filled with liquid reaction mixture that protected it from contacting with air at the following testing steps. The testing conditions: P_{H_2} = 30 atm, T = 100 °C, catalyst loading 0.2 g, reaction mixture – 0.3 g of PCAP in 12 ml of Pr^iOH, reaction time τ = 5–12 h needed for keeping the PCAP conversion in the range of 10–30%. The reaction rate was calculated as V [mmol (g cat.)$^{-1}$ h^{-1}] = $= [(10^3 \times 0.3/MW)X]/w\tau$, where X is PCAP conversion, MW is PCAP molecular weight, and w is catalyst weight (g). The contents of residual PCAP and its hydrogenation products were analyzed by GC [an HP-6890 instrument equipped with FID employing a capillary DB-WAX column (30 m, i.d. = 0.25 μm) and He as a carrier gas]. 2-Methoxyethyl ether was used as an internal standard. The selectivity for 1-(*p*-chlorophenyl)ethanol (hydrogenation route) and acetophenone (hydrodechlorination route) was calculated based on the concentrations of these compounds found in the products mixture by GC analysis.

© 2011 Mendeleev Communications. All rights reserved.

Table 1 Preparation methods and characteristics of Ni/MWCNT materials.

Sample	Preparation procedure	Characteristics of catalytic materials				
		Total surface area/ m^2 g^{-1}	Nickel content (wt%)		Nickel crystal size/nm	Estimated specific surface area of Ni^0 phase/m^2 per g Ni
			Chemical analysis (total Ni)	Phase analysis (Ni^0)		
S1	CNT produced by direct injection method (parent CNT)	204	6.1	6	30	1.3
S2	Carboxylation of CNT followed by treatment with nickel acetate and H_2-reduction at 550 °C	197	10.5	11	20	3.7
S3	Carboxylation of CNT followed by treatment with nickel formate and H_2-reduction at 550 °C	148	33.5	27	35	5.2
S4	Carboxylation of CNT followed by treatment with nickel acetate and reduction with hydrazine hydrate at room temperature	203	9.5	—	—	—
S5	Deposition of nickel by ultrasonication of CNT suspension in $Ni(CO)_4$ solution in decaline	163	24.6	26	4	41.4
S6	Deposition of nickel by ultrasonication of CNT suspension in $Ni(CO)_4$ solution in decaline	138	51.3	50	8	43.1
S7	Impregnation with $Ni(NO_3)_2$ solution heating at 350 °C, H_2-reduction at 550 °C	184	15.0	15	22	4.6

of 20 nm (XRD, Table 1). During the synthesis, the protons of surface carboxylic groups were replaced by Ni^{2+} ions.[20,21] Then, these ions acted as specific nucleation sites for well-dispersed nickel hydroxide, which was converted into metal under reduction.[11] Due to chemical interaction with surface carboxylic groups the nickel ions and nickel hydroxide were reduced at higher temperatures than pure NiO. This was reflected by a shift of the main maximum in the TPR spectra from 500 to 550 °C and the appearance of an additional shoulder at higher reduction time (Figure 3, curve *4*). XRD (Figure 2, curve *3*) revealed in the reduced sample S2 only one nickel-containing phase – metal nanocrystals, located exclusively at the outer surface of MWCNTs. Occlusion of nickel precursor aqueous solution inside hydrophobic CNT channels was, likely, hampered.[22,23]

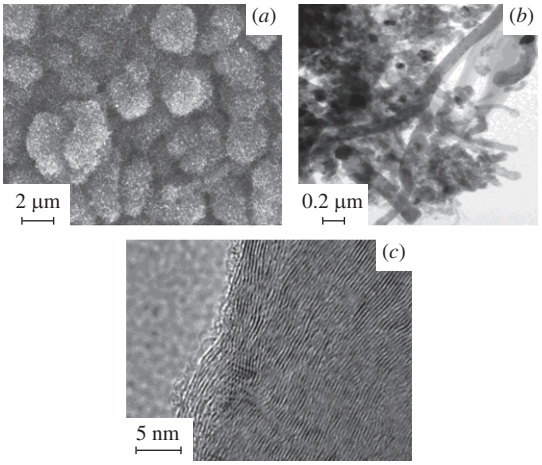

Figure 1 Micrographs of parent MWCNTs prepared by a direct injection method: (*a*) microspherical bundles of MWCNTs (SEM); (*b*) residual Ni^0 and NiO nanoparticles inside the MWCNT bundles (TEM); and (*c*) graphene layers constituting the MWCNT structure (HRTEM).

Implementation of nickel formate instead of acetate yielded material (sample S3) with a metal loading higher by a factor of ~3 (Table 1) as a result of sonication at metal deposition step. A comparison of the nickel contents measured by chemical and XRD phase analysis revealed the conversion of nickel into metal nanocrystals (Ni^0) with an average size of 35 nm at 80% – residual NiO was found on XRD spectrum (Figure 2, curve *4*). The nickel reduction with hydrazine hydrate (sample S4) did not yield a metallic phase since the presence of low reducible $NiCl_2$ and $Ni(OH)_2$.

The sonochemical deposition of nickel from a solution of $Ni(CO)_4$ in decaline yielded materials with 25 and 51 wt% nickel contents (samples S5 and S6, respectively) (Table 1). According to XRD data, nickel existed only as a metallic phase (Figure 2,

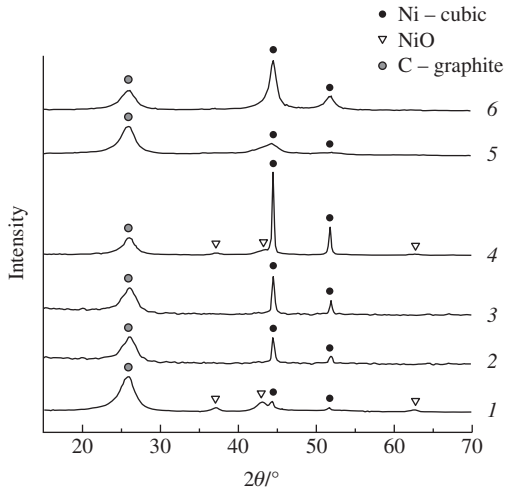

Figure 2 XRD patterns of Ni/MWCNT materials: (*1*) parent CNT, (*2*) parent CNT after H_2-reduction at 550 °C, S1; (*3*) material S2 after H_2-reduction; (*4*) material S3 after H_2-reduction; (*5*) material S5; and (*6*) material S6.

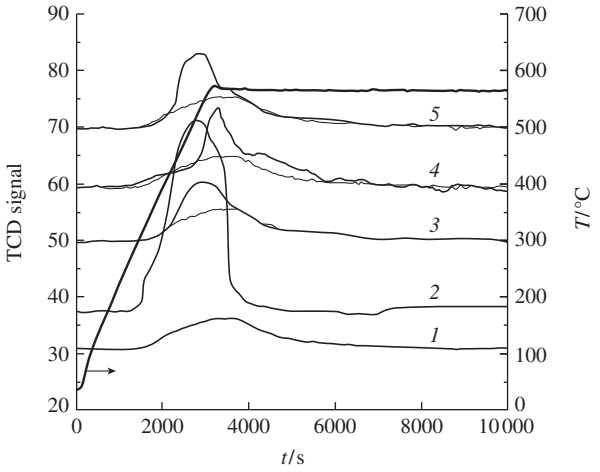

Figure 3 TPR spectra of reference materials and MWCNT decorated with different metallic nickel precursors: (*1*) parent CNT after nickel extraction; (*2*) NiO; (*3*) parent CNT, S1; (*4*) material S2; and (*5*) material S7.

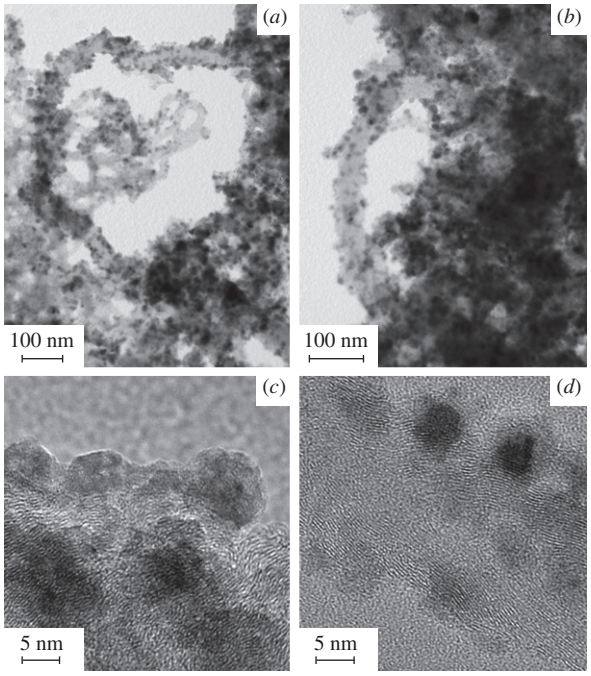

Figure 4 TEM micrographs of materials obtained by the sonochemical decoration of MWCNTs: general view of (*a*) S5 and (*b*) S6; (*c*), (*d*) Ni^0 nanocrystals partially embedded in graphite walls at the external MWCNT surface (S5).

curves *5*, *6*). The average crystal sizes were 4 and 8 nm in samples S5 and S6, respectively. So small values were never reported before for MWCNTs decorated with nickel nanocrystals at loadings of > 10 wt%. HRTEM data [Figure 4(*a*),(*b*)] show that nickel nanoparticles in these materials are uniformly distributed at the external surface of tubes as individual crystals or their aggregates. HRTEM images of material S5 demonstrate a narrow size distribution, consistent with the values calculated from XRD data [Figure 4(*c*),(*d*)]. Nanocrystals were partially embedded in the graphite body of CNT walls, that, probably, stabilized them against sintering and partially decreased surface area of nickel relative to the value calculated based on the nickel crystal size. Procedure described did not change the pore size distribution (PSD) mode (Figure 5): decreasing of the integral intensity for D = 4 nm peak is proportional to the metal loading, which supports the conclusion that nickel nanoparticles are located only at the external surface of MWCNTs, since the absolute channels volume, as well as shape and position of peaks in PSD spectra, remain the same. On the contrary, the shape and integral intensity of a wide peak at D = 4–10 nm changes significantly after insertion of nickel.

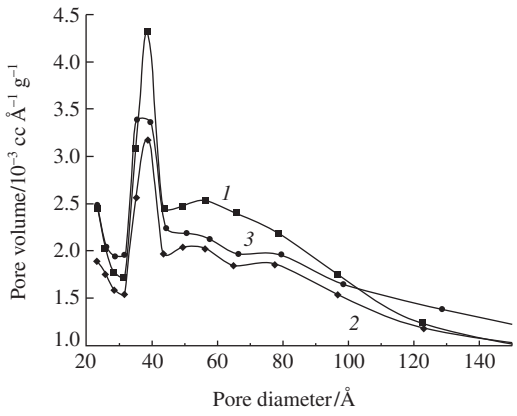

Figure 5 Pore size distribution in starting MWCNT (*1*) after nickel extraction and in materials (*2*) S5 and (*3*) S6 obtained by the sonochemical deposition of metallic nickel.

It means that the volume of these mesopores became partially filled with metal nanoparticles decorating the external surface of MWCNTs. This correlates with decreasing surface area in the Ni/MWCNT composites from 204 to 163 (S5) and then to 138 $m^2\ g^{-1}$ (S6) after insertion of increased amounts of nickel (Table 1).

XRD data show only a NiO phase after thermal decomposition at 350 °C of nickel nitrate, deposited in pores of MWCNTs, in sample S7. The TPR spectrum of the material is similar to that recorded for starting MWCNT (Figure 3, curve *5*). The average nickel crystal size after reduction was estimated at 18 nm, the nickel content was 15 wt% (Table 1).

The effect of MWCNT decorating strategy with nickel nanocrystals on the catalytic performance of Ni/CNT catalysts was evaluated by comparative testing the activity and selectivity of materials (samples S1–S3, S5–S7) in the hydrogenation of *p*-chloroacetophenone (PCAP). The use of the latter as a substrate for catalytic experiments allowed us to estimate the hydrodechlorination and hydrogenation functions of the prepared catalytic materials.[24] The main products of PCAP conversion with all tested Ni/MWCNT catalysts were 1-(*p*-chlorophenyl)-ethanol and acetophenone (Table 2). High selectivity for the first product could be achieved without implementation of basic additives[25,26] or addition of a second metallic component[27,28] for depressing undesirable side reactions. In contrast to a Pd/CNT catalyst yielding complete hydrodechlorination of halobenzenes under mild conditions,[29] Ni/MWCNT in the present study displayed high, up to ~70%, selectivity for the hydrogenation of the carbonyl group.

Dispersion and loading of metallic nickel phase decorating MWCNTs has a strong impact on the hydrogenation activity of tested catalytic materials (Table 2). It increases with raising the surface area of metallic nickel phase‡ (Table 1). The direct sonochemical deposition strategy, as expected, yielded materials S5 and S6 with the highest catalytic activity. The total rate of PCAP conversion normalized per gram of catalyst, as well as specific reaction rate per gram of active nickel component measured with materials S5 and S6 were 2–18 times higher, as compared with catalysts S1–S3 and S7 prepared by the reduction of oxide nickel precursors. The measured total rate of PCAP conversion was nearly proportional to the estimated surface area of metallic nickel phase for materials with low surface area of metallic nickel, samples S1–S3, S7 (Tables 1 and 2). In materials prepared by sonochemical deposition, the increase in the metallic nickel surface area by about an order of magnitude (from 4.6–5.3 $m^2\ g^{-1}$ Ni in samples S3, S7 to 41.4–43.1 $m^2\ g^{-1}$ Ni in samples S5, S6) (Table 1) led to a substantially lower increase in the PCAP hydro-

Table 2 Testing of Ni/MWCNT catalysts in the hydrogenation of PCAP.[a]

Catalyst	PCAP hydrogenation rate		PCAP hydrogenation selectivity (%)	
	mmol $(g\ cat)^{-1}\ h^{-1}$	mmol $(g\ Ni)^{-1}\ h^{-1}$	1-(*p*-Chlorophenyl)ethanol	Acetophenone
S1	0.013	0.210	69.6	27.3
S2	0.055	0.520	69.8	20.2
S3	0.122	0.360	64.2	19.3
S5	0.228	0.912	67.2	15.6
S6	0.234	0.468	69.2	21.0
S7	0.077	0.510	67.6	19.4

[a]Testing conditions: batch reactor; T = 100 °C, P_{H_2} = 30 atm, t = 3–20 h; catalyst loading, 0.1–0.5 g; PCAP conversion, 5–30%; starting reaction mixture: 0.3 g PCAP in 12 ml of Pr^iOH.

‡ Estimated as $S_{Ni} = (6000/\rho d)x$, where ρ is theoretical density of cubic nickel phase, d is its average crystals size and x is the concentration of metallic nickel based on phase analysis.

genation rate, from 77–122 to 228–234×10^{-3} mmol (g cat.)$^{-1}$ h^{-1} (Table 2). Since diffusion limitations should be excluded from consideration (small catalysts particles size, high agitation speed) this occurrence can be realized as a result of partial exposure of the surface of metallic nickel particles to the PCAP reacting molecules because of partial embedding of nickel nanocrystals in MWCNT walls on the external surface [Figure 4(*c*),(*d*)]. Both phenomena lead to a partial screening of the surface of nickel nanoparticles. Nevertheless, the direct sonochemical decoration strategy excludes a high-temperature reduction of oxide phase and produces material with catalytic activity much higher than that provided by other decoration approaches, leading to a wide metal size distribution of 20–35 nm at low loadings of 6–10 wt%.

Decoration of MWCNTs with nickel nanocrystals by direct sonochemical deposition as a result of *in situ* decomposition of carbonyl precursor significantly increases the dispersion and uniformity of size distribution of metallic phase at high loadings: the average crystal size of 4–8 nm at 25–50 wt% nickel content, which enhances the catalytic activity of the material in the selective hydrogenation of chloroacetophenone by factors of 2–18, comparing with traditional decoration methods.

This study was supported by a joint MSTI-RFBR programme: grant nos. 3-3549, 3-5739 (Israel Ministry of Science and Technology), 09-03-92482 and 06-03-72032 (Russian Foundation for Basic Research). We are grateful to A. S. Mikheykina for her assistance in catalytic experiments and to Dr. A. Erenburg and Dr. V. Ezersky for performing material characterizations by XRD and HRTEM.

References

1 L. M. Ang, T. S. A. Hor, G. Q. Xu, C. H. Tung, S. P. Zhao and J. L. S. Wang, *Carbon*, 2000, **38**, 363.
2 C. Pham-Huu, N. Keller, V. V. Roddatis, G. Mestl, R. Schlögl and M. J. Ledoux, *Phys. Chem. Chem. Phys*., 2002, **4**, 514.
3 E. Unger, G. S. Duesberg, M. Liebau, A. P. Graham, R. Seidel, F. Kreupl and W. Hoenlein, *Appl. Phys. A*, 2003, **77**, 735.
4 P. Ayala, F. L. Freire, L. Gu, D. G. Smith, I. G. Solorzano, D. W. Macedo, J. B. Vander Sande, H. Terrones, J. Rodriguez-Manzo and M. Terrones, *Chem. Phys. Lett*., 2006, **431**, 104.
5 C. Bittencourt, A. Felten, J. Ghijsen, J. Pireaux, W. Drube, R. Erni and G.Van Tendeloo, *Chem. Phys. Lett*., 2007, **436**, 368.
6 C.-T. Hsieh, Y. W. Chou and W.-Y. Chen, *J. Solid State Electrochem.*, 2008, **12**, 663.
7 J. P. Cheng, X. B. Zhang and Y. Ye, *J. Mater. Process. Technol.*, 2008, **206**, 180.
8 Y. Tang, D. Yang, F. Qin, J. Hu, C. Wang and H. Xu, *J. Solid State Chem*., 2009, **182**, 2279.
9 X. Wang, F. Zhang, X. Zhu, B. Xia, J. Chen, S. Qiu and J. Li, *J. Colloid Interface Sci*., 2009, **337**, 272.
10 Y. Lin, K. A.Watson, M. J. Fallbach, S. Ghose, J. G. Smith, D. M. Delozier, W. Cao, R. E. Crooks and J. W. Connel, *ACS NANO*, 2009, **3**, 871.
11 Y. Cao, Q. Jiao, H. Liu, X. Tang and Y. Zhao, *Physica E*, 2009, **41**, 1824.
12 A. S. Adekunle and K. I. Ozoemena, *J. Electroanal. Chem.*, 2010, **645**, 41.
13 H. Zhaoa, X. Hana, M. Hana, L. Zhang and P. Xu, *Mater. Sci. Eng. B*, 2010, **167**, 1.
14 H. Wu, C. Qian, Y. Cao, P. Cao, W. Li, X. Zhang and X. Wei, *J. Phys. Chem. Solids*, 2010, **71**, 290.
15 P. Azadi, R. Farnood and E. Meier, *J. Phys. Chem. A*, 2010, **114**, 3962.
16 J. Gomez, Y. Verde, J. Lara-Romero and G. Alonso-Ninez, *Fullerenes Nanotubes Carbon Nanostruct*., 2009, **17**, 507.
17 X. Zhao, P. Jiang and S. Xie, *Solid State Commun.*, 2009, **149**, 1984.
18 J.-P. Tessonnier, O. Ersen, G. Weinberg, C. Pham-Huu, D. S. Su and R. Schlögl, *ACS NANO*, 2009, **3**, 2081.
19 M. N. Kirikova, A. S. Ivanov, S. V. Savilov and V. V. Lunin, *Izv. Akad. Nauk, Ser. Khim.*, 2008, 291 (*Russ. Chem. Bull., Int. Ed.*, 2008, **57**, 298).
20 T. W. Ebbsen, H. Hiura, M. E. Bisher, M. M. J. Treacy and J. L. Shreeve-Keyer, *Adv. Mater.*, 1996, **8**, 155.
21 B. He, M. Wang, W. Sun and Z. Shen, *Mater. Chem. Phys*., 2006, **95**, 289.
22 H. Ma, L. Wang, L. Chen, C. Dong, W. Yu, T. Huang and Y. Qian, *Catal. Commun.*, 2007, **8**, 452.
23 O. Ersen, J. Werckmann, M. Houlle, M. J. Ledoux and C. Pham-Huu, *Nano Lett.*, 2007, **7**, 1898.
24 H.-U. Blaser, C. Malan, B. Pugin, F. Spindler, H. Steiner and M. Studer, *Adv. Synth. Catal.*, 2003, **345**, 103.
25 K. Hattori, H. Sajiki and K. Hirota, *Tetrahedron*, 2001, **57**, 4817.
26 R. V. Malyala, C. V. Rode, M. Arai, S. G. Hegde and R. V. Chaudari, *Appl. Catal., A*, 2000, **193**, 71.
27 M. Casagrande, L. Storato, A. Talon, M. Lenarda, M. Fratini, E. Rodrigues-Cawstellon and P. Maireles-Torres, *J. Mol. Catal. A: Chem.*, 2000, **188**, 133.
28 J. Masson, P. Cividino and J. Court, *Appl. Catal., A*, 1997, **161**, 191.
29 X. Wang, L. Chen and K. Yang, *Chinese Pat. Appl.*, 2009, No. CN 101455889 A20090617.

Received: 4th November 2010; Com. 10/3625